Int J Thermophys (2008) 29:764–786
DOI 10.1007/s10765-008-0422-0

Detection of Melting Temperatures and Sources of Errors Using Two-Color Pyrometry During In-flight Measurements of Atmospheric Plasma-Sprayed Particles

Georg Mauer · Robert Vaßen · Detlev Stöver

Received: 18 September 2007 / Accepted: 11 March 2008 / Published online: 10 April 2008

Abstract Growing demands on the quality of plasma-sprayed coatings require reliable methods to monitor and optimize the spraying processes. As the coating microstructures are dependent on the characteristics of the powder feedstock, particle in-flight diagnostics is of great importance. In particular, the melting status of the particles is critical in this regard. Thus, the accurate determination of the particle temperature is necessary. In-flight particle temperature measurements during atmospheric plasma spraying (APS) of tungsten, molybdenum, and yttria-stabilized zirconia by two-color pyrometry were analyzed statistically. The diagnostic tool applied is the DPV-2000 (Tecnar). The particle temperature distributions allow for assessment of the melting status of the particles as well as the identification of the melting temperature and particle fractions in the molten and solidification state. Furthermore, the relevant systematic and material-dependent sources for measurement errors using two-color pyrometry were investigated. Their influence was carefully estimated and corrected. As long as there are reliable data available on the emissivity of the powder material, good agreement between the corrected measured melting temperatures and the reference data can be expected.

Keywords Diagnostics · Particle characteristics · Plasma spraying · Two-color pyrometry

1 Introduction

Growing demands on the quality of plasma-sprayed coatings require reliable methods to monitor and optimize the spraying processes. As the coating microstructures are

G. Mauer (✉) · R. Vaßen · D. Stöver
Institut für Energieforschung (IEF-1), Forschungszentrum Jülich GmbH, 52425 Jülich, Germany
e-mail: g.mauer@fz-juelich.de

dependent on the characteristics of the powder feedstock, particle in-flight diagnostics is of great importance. In particular, the melting status of the particles is critical in this regard. Thus, the accurate determination of the particle temperature is necessary. In the following, the detection of the material-specific melting temperature is shown based on single-particle in-flight measurements by two-color pyrometry during atmospheric plasma spraying. The diagnostic system applied is the DPV-2000. Furthermore, systematic and material-dependent sources of error were investigated.

2 Fundamentals of Temperature Measurement by Two-Color Pyrometry

Particle temperature measurement based on two-color pyrometry involves filtering of the thermal radiance emitted by a particle at two wavelength bands [1]. In case of the DPV-2000, the wavelengths are at $\lambda_1 = (787 \pm 25)\,\mathrm{nm}$ and $\lambda_2 = (995 \pm 25)\,\mathrm{nm}$. Wien's approximation of Planck's law which describes the spectral radiation density of a blackbody is used to determine the particle temperature at the applied wavelengths.

The emissivity, ε, gives the deviation of the radiation performance of a real body compared to an ideal blackbody. Values of ε vary between zero to unity and, in principle, depend on the wavelength and temperature. Because the emissivities are unknown for many applications, the gray body assumption $\varepsilon(\lambda_1)/\varepsilon(\lambda_2) = 1$ is used where it is hypothesized that the emissivity is not dependent on the wavelength. However, as shown below, in many cases this assumption is not fulfilled so that a systematic error is introduced which can lead to significant temperature deviations.

3 Experimental

One of the particle diagnostic systems, the atmospheric plasma spray facilities are equipped with at the Institute of Energy Research (IEF-1), Forschungszentrum Jülich GmbH, Germany, is the DPV-2000 (TECNAR Automation Ltd., St-Bruno, QC, Canada). It enables the measurement of particle velocities, temperatures, and diameters. The velocity is determined by measuring the time between two signals triggered by a radiating particle passing the two-slit mask of the optoelectronic sensor head. In conjunction with the distance of the slits and the magnification factor of the lens, the velocity can be calculated. The temperature, on the other hand, is acquired by two-color pyrometry, as previously described, while the diameter can be obtained from the radiation energy emitted at a single wavelength with the assumption that the melted particles are approximately spherical. However, this measurement has to be calibrated by means of a powder of known particle size distribution and having the same radiation characteristics as the particles to be investigated. Most of the time, since the measurement volume is relatively small ($<1\,\mathrm{mm}^3$), only single particles are evaluated. Thus, the data is collected for individual particles and can be subsequently analyzed statistically.

A typical measurement procedure is as follows. The plasma gun is positioned in front of the optoelectronic sensor of the DPV-2000 so that the measurement scope is within the spraying distance of the work piece. This measuring head collecting the

particle radiation is mounted on a scanning unit which moves it perpendicularly to the gun axis. Before each measurement, the particle flow is scanned along the horizontal and vertical directions to determine the point of maximum particle flow rate. This is done by a two-step procedure with increasing resolution. Finally, the precise position for measurement is determined at this point. Positioning accuracy is at ± 0.1 mm. Investigation of particles at certain measurement times is necessary to support the mean and standard deviations by a sufficient number of individual particle data. In this work, data sets of approximately 5000 particles were each recorded for about 30 s.

In-flight measurements of particle temperatures were carried out on a multicoat facility (Sulzer Metco, Wohlen, Switzerland) with atmospheric plasma spraying using a three-cathode Triplex II gun mounted on a six-axis robot. Due to the three-cathode concept, arc fluctuations of this gun are much smaller than what are expected for typical one-cathode torches. The spraying parameters are listed in Table 1. The actual values were monitored and recorded continuously during the process. Typical standard deviations of the parameters were found to be 1 A current, 0.1 V voltage, 0.1 standard liters per minute carrier and plasma gas flows, and 1.2% rotational speed of the powder dosing disk.

The powder characteristics are given in Table 2. The metal powders are not typically sprayed by atmospheric plasma spraying. However, they have been chosen because there are reliable data for their emissivities and they are not semi-transparent. Powders were taken only from one lot, and were previously characterized prior to experimentation. Characterization involved scanning electron microscopy, x-ray crystallography,

Table 1 Spraying parameters for in-flight measurements of particle temperatures

Plasma gun	Triplex II
Current	300/520 A (varied)
Plasma gas	50 slpm Ar, 4 slpm He
Carrier gas	1.6 slpm Ar
Stand-off distance	100/175 mm (varied)

Table 2 Characteristics of applied powder feedstock material

Powder	Tungsten		Molybdenum	8% Yttria-stabilized zirconia (YSZ)
	Coarse	Fine		
Supplier	H.C. Starck	H.C. Starck	Plasma-Technik	Sulzer
Product	Amperit 140.2	Amperit 140.3	AMDRY 3418	Metco 204NS
Morphology	Sintered/Crushed	Sintered/Crushed	Sintered/Crushed	Spheroidal (HOSP process)
d_{10} (μm)	37	7	17	25
d_{50} (μm)	69	26	76	57
d_{90} (μm)	123	45	123	101

laser diffraction, and the determination of true, bulk, and knock densities. The 10%, 50%, and 90% diameters given in Table 2 were measured by laser diffraction and not by in-flight particle diagnostics. The diagnostic measurements of each powder were performed in direct sequence without refilling the powder feed units. Thus, it can be expected that comparable measurement results will be achieved regarding the particle size and shape distributions from one experiment to another.

4 Measured Density Distributions of In-flight Particle Temperatures

4.1 Results and Discussion

Figure 1 shows the particle temperature distributions for the coarse tungsten powder measured at a spraying distance of 100 mm. Each distribution contains at least 5000 single particle data. Various input power levels were achieved by setting the current between 300 A and 520 A. It is found that the distributions are bimodal in the medium power range. The frequency distributions contain two fractions, one at a constant mean temperature, and another at a mean temperature being variable with the power. According to that, the measured particle temperature distributions can be approximated by one or two Gaussian normal distribution functions, respectively. The normal distribution approximating the fraction at constant mean temperature is indicated by distribution A, while the other one at variable mean temperatures is indicated by distribution B. In case of bimodal distributions, in the following the sum of both is referred to as the total distribution.

The approximation of the normal distribution functions can be represented by their mean temperatures and by their portion of the particle totality, which corresponds to the area under the distribution curves, i.e., to its integral. In case of unimodal distributions, the portion is set to 100%, while for bimodal distributions, the sum of both the portions yields 100%. Drawing these portions as a function of their mean temperatures, gives the plot shown in Fig. 2. The constant temperature level of one particle portion and the variable mean temperatures of the other portion are distinct.

Based on this, it is assumed that the mean temperature of the partial particle temperature distribution A at a constant level is the melting temperature of the powder feedstock material. Since the particles are cooling when approaching the substrate, their fusion enthalpy is released when the melting/solidifying temperature is reached. As this takes time, the residence probability of the particle at melting temperature is larger than at other temperatures below or above the melting point. However, the peak of the normal distribution at constant mean temperature was measured at approximately 2930°C, whereas the melting temperature of tungsten is 3410°C. Below is the discussion on whether this deviation can be explained by systematic or material-dependent measurement errors by two-color pyrometry.

Similar measurements and analyses of YSZ are reported in [2]. Here, it is also stated that the temperature distributions provide information on the melting status of the particles. One portion of the particles was found to have the same mean temperature at various spraying parameters. Different particle morphologies were reported to give similar peaks at the same temperature. This may indicate that after melting the

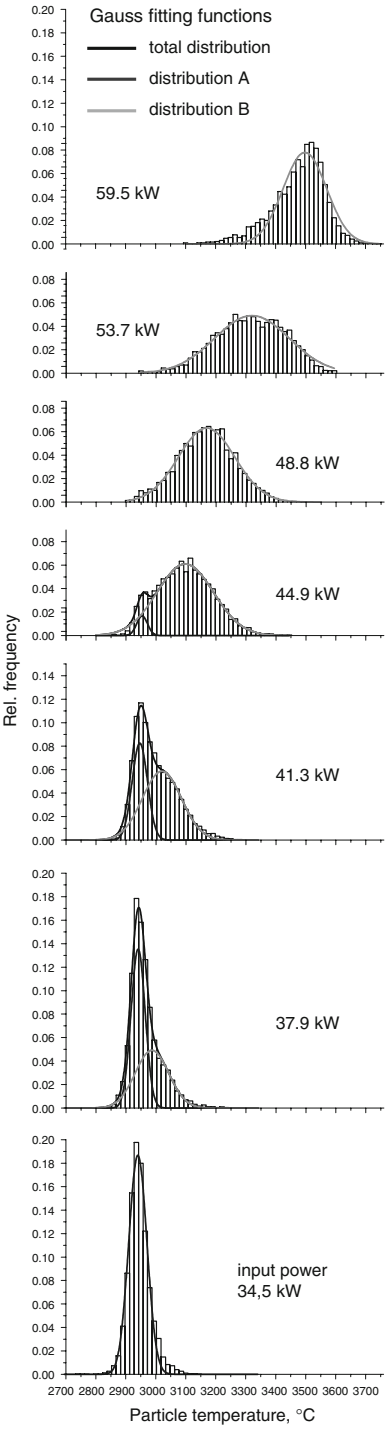

Fig. 1 Particle temperature distributions for the coarse tungsten powder measured at a spraying distance of 100 mm

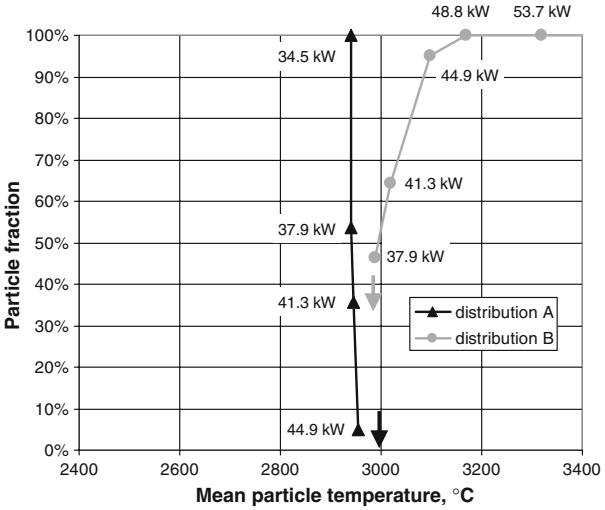

Fig. 2 Particle fractions as a function of their mean temperature for the coarse tungsten powder measured at a spraying distance of 100 mm

liquid particles have similar characteristics, and that the constant peak temperature may be related to the melting temperature. Likewise, there are discrepancies between the measured and the referenced melting temperatures which are explained by the limited measurement accuracy of the diagnostic system, which was the same as used in the experiments described here.

To prove the hypothesis stated above, several measurements were carried out and evaluated. Based on the initial experiment, the stand-off distance, the particle size distribution, and the powder materials were varied.

Figure 3 shows particle temperature distributions of the same coarse tungsten powder at identical power levels as the previous experiment, but at an enlarged spraying distance of 175 mm. The corresponding plot of the particle portions at the same and variable mean temperatures is given in Fig. 4. The constant temperature peak is almost at the same temperature as that measured at a shorter spraying distance of 100 mm. This proves that this temperature is characteristic for the powder feedstock material. The other particle fraction plot is moved to lower temperature which is plausible for the enlargement of the stand-off distance. Figure 5 shows the results for the fine tungsten powder using the same process parameters as the coarse tungsten powder. Again, the particle portion at constant peak temperature is located at almost the same temperature as that of the coarse tungsten powder.

Figures 4 and 5 show that the distribution plots of the particles with variable mean temperatures intersect the courses of the constant temperature peaks. One explanation for this phenomenon is superficial undercooling. As shown in [3] for alumina droplets heated by a laser beam and subsequently cooling freely in an aerodynamic levitation device, the measured surface temperature drops below the melting temperature. In the case of alumina this decline was approximately 240 K. When the retarded solidification starts, temperature is increasing again due to the released fusion enthalpy and

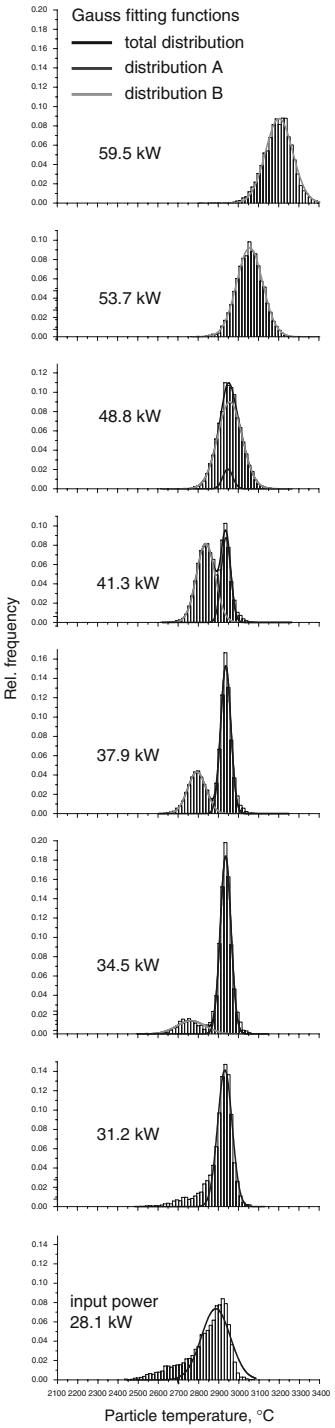

Fig. 3 Particle temperature distributions for the coarse tungsten powder measured at a spraying distance of 175 mm

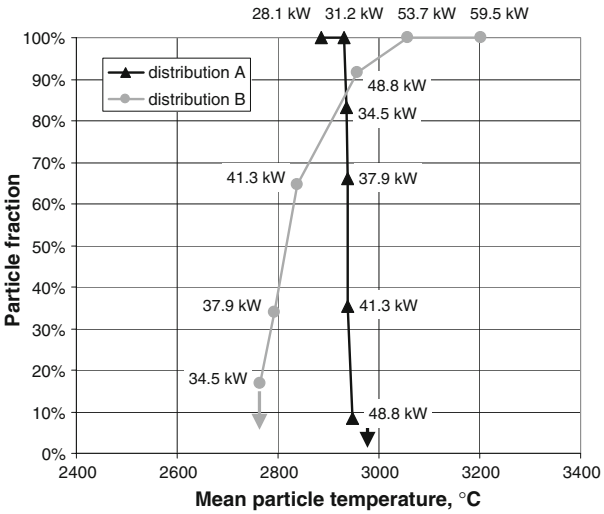

Fig. 4 Particle fractions as a function of their mean temperature for the coarse tungsten powder measured at a spraying distance of 175 mm

Fig. 5 Particle fractions at constant and variable temperatures versus their mean temperature for the fine tungsten powder measured at a spraying distance of 175 mm

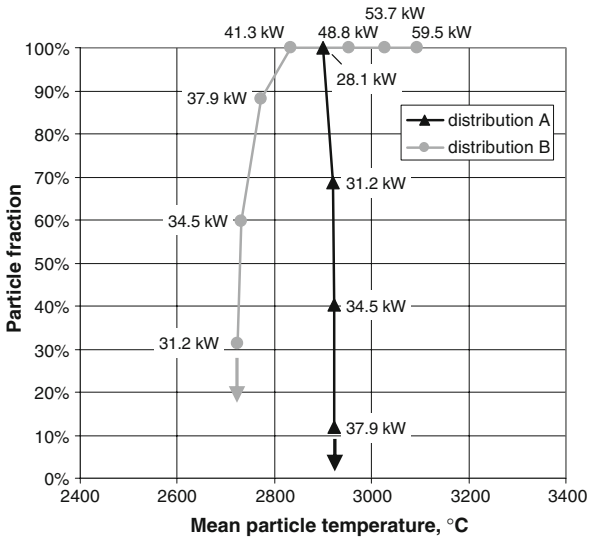

remains at the melting temperature until the solidification is completed. Thus, taking into account such supercooling effects, the intersecting plots of the particle fractions against the mean temperatures can be justified. Other possible reasons may be heat loss due to surface evaporation, or in the case of metals surface oxidation of the molten material and subsequent variation of emissivity.

Figures 6 and 7 show the results of similar measurements carried out on molybdenum powder. Again, two particle fractions can be identified, even though the location of the particle fraction peak at constant level is not as stable as that of the tungsten

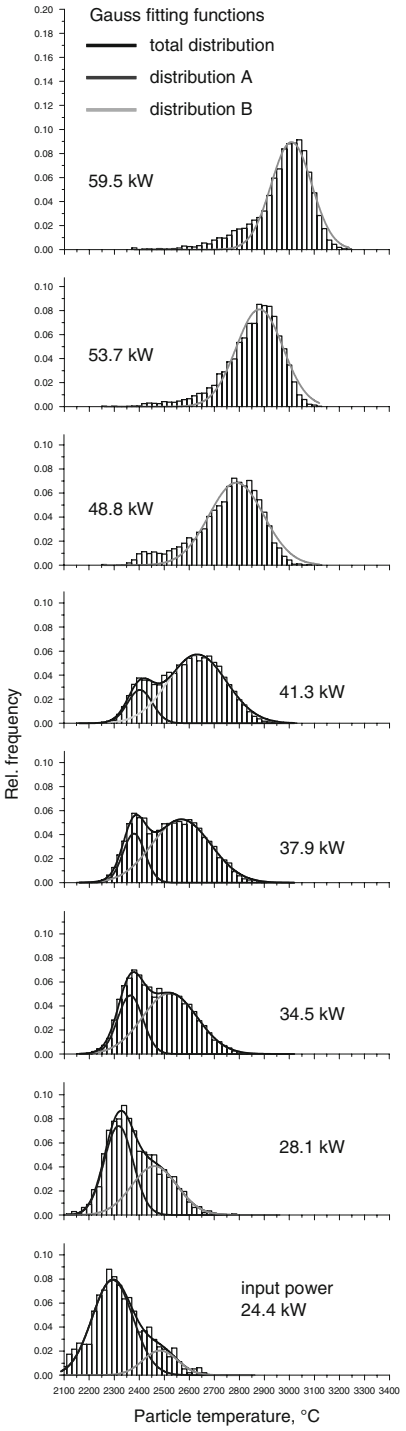

Fig. 6 Particle temperature distributions for the molybdenum powder measured at a spraying distance of 175 mm

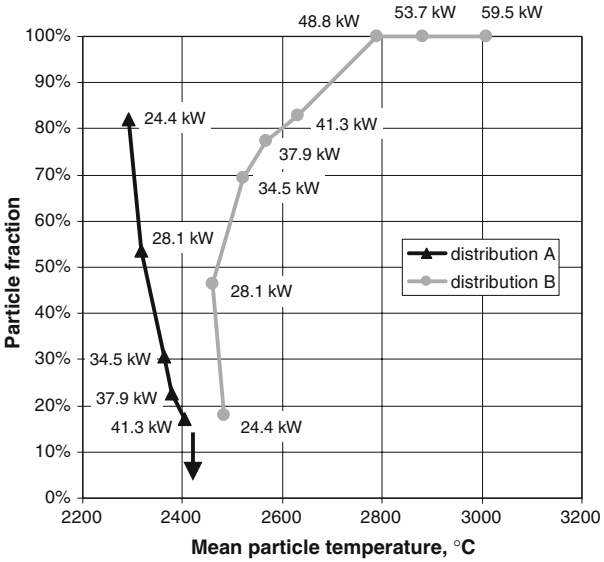

Fig. 7 Particle fractions at constant and variable temperatures versus their mean temperature for the molybdenum powder measured at a spraying distance of 175 mm

powders. Its measured mean temperature of 2340°C is also below the melting temperature of molybdenum which is 2610°C.

Figures 8 and 9 show the diagnostic results for the yttria-stabilized zirconia powder at 175 mm stand-off distance. As the different particle fractions show similar values of the mean temperatures, the Gauss approximation algorithm becomes less selective. As a consequence, the development of the plots in Fig. 9 becomes irregular, resulting from discontinuous data plots. Therefore, the data points are plotted without linking lines. In contrast to the previous results, particle fractions which have already completely solidified again can be identified as well. Their portion was found to increase with decreasing plasma power.

As described above, it is also possible to approximate the particle diameter from the emitted radiation energy by means of the DPV-2000. Also, if there is no powder available with a known diameter distribution and the same radiation characteristics for calibration purposes, nevertheless, correlations can be based on diameters. Thus, regarding the different particle portions, the difference in their mean diameters can be determined by evaluating single particle data. For each of the previously described experiments, these differences in mean particle diameters were found to be of significant magnitudes. The solidifying particles forming the fraction peak at melting temperature were always larger, on average, than the still-liquid particles at variable temperatures. This shows that particles of different sizes have different trajectories and therefore, different thermal cycles. Larger particles are heated to low temperatures only as compared to the smaller ones, due to their lower trajectory. Furthermore, they have larger thermal masses. As a consequence, they also re-solidify earlier.

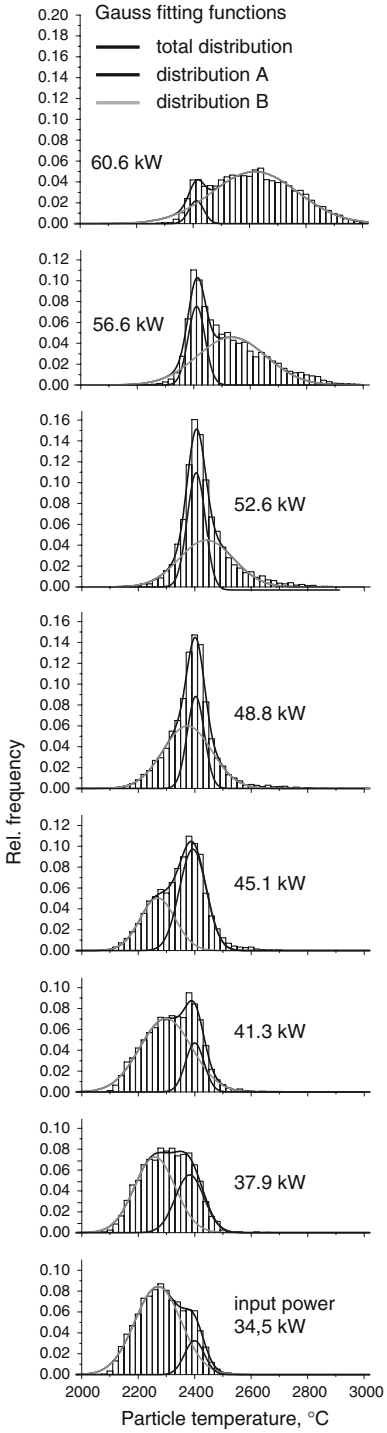

Fig. 8 Particle temperature distributions for the YSZ powder measured at a spraying distance of 175 mm

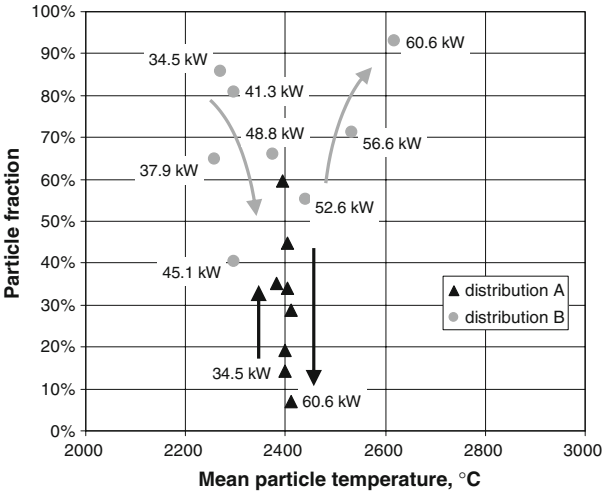

Fig. 9 Particle fractions at constant and variable temperatures versus their mean temperature for the YSZ powder measured at a spraying distance of 175 mm

4.2 Sources of Errors Using Two-Color Pyrometry for In-flight Particle Measurements

4.2.1 Emissivity Characteristics of Measured Powder Materials

As described above, the emissivity ratio of the measured powder materials is of importance for accurate two-color pyrometry measurements. Generally, there are more data in the literature on the emissivity of metals in the visible and near-IR range at high temperatures than that of other materials. One reason is that these data are needed for precise temperature measurements in metal working. For oxide ceramics, however, emissivity data are almost available only for low temperatures and large wavelengths, since the focus is on the thermal load capacity of component parts.

Figure 10 shows the temperature-dependent impact of the emissivity ratio $\varepsilon(\lambda_1)/\varepsilon(\lambda_2)$ varying from unity, on the resulting temperature measurement error. It is obvious that deviations from the gray-body assumption cause systematic measurement errors reaching up to some hundred K at higher temperatures.

In the following sections, the emissivity characteristics of tungsten and molybdenum are introduced as examples for metals, while yttria-stabilized zirconia is an example for oxide ceramics.

4.2.1.1 Tungsten The experimental data on normal spectral emissivities of solid and liquid tungsten are reported at wavelengths of 684.5 nm, 902 nm, and 1570 nm in the temperature range between 3000 K and 4800 K [4]. The values show a less distinctive dependence on temperature, but obviously impacted by the wavelength. At the solid-to-liquid phase transition, the emissivity evolutions show a noticeable downwards step. This effect is due to changes on two optical emission mechanisms, namely, intra- and

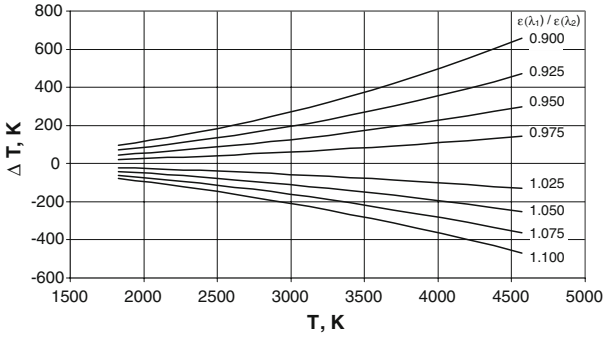

Fig. 10 Temperature measurement error dependent on the exact temperature for a set of emissivity ratios different from unity

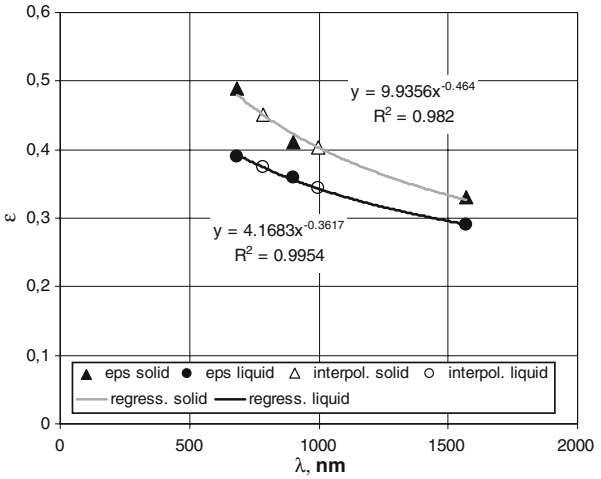

Fig. 11 Measured emissivity values taken from [4] (*filled circles*), regression functions (*black and gray lines*), and interpolated values at filtering wavelengths of DPV-2000 (*open circles*) for each of the solid and liquid phases of tungsten (eps means ε)

inter-band transitions [5]. Figure 11 shows three emissivity values for each of the solid and liquid phases, averaging the merely small temperature dependence. These values were interpolated as a function of the wavelength by a regression function in the form of $\varepsilon(\lambda) = a\lambda^b$ where a and b are the regression coefficients and λ is the wavelength in nm. This expression refers to the Hagen-Rubens law in a more general form [6], where b is set to -0.5 for metals. The fitting of the regression function resulted in the coefficient values of $a = 9.9356$ and $b = -0.464$ for the solid tungsten. With this regression function, the emissivity was interpolated at the two wavelengths which were used for the two-color pyrometry by the DPV-2000. For solid tungsten, these emissivities are 0.45 at $\lambda_1 = 787\,\text{nm}$ and 0.40 at $\lambda_2 = 995\,\text{nm}$. The emissivity ratio is 1.12 showing some deviation from the gray-body assumption. For the liquid phase, the regression coefficients are $a = 4.1683$ and $b = -0.3617$ giving emissivities of

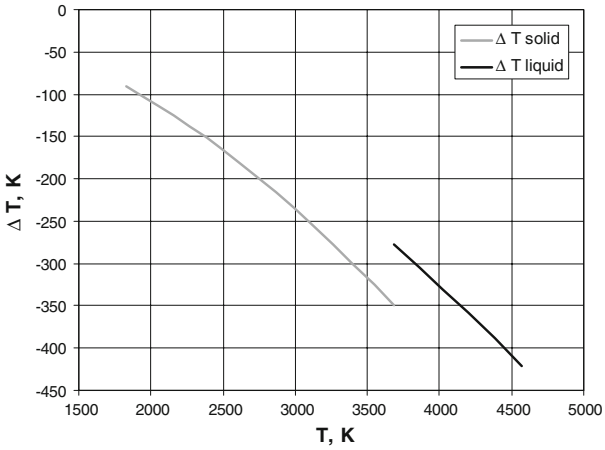

Fig. 12 Temperature measurement error caused by the deviation from the gray-body assumption for solid and liquid tungsten

0.37 at $\lambda_1 = 787$ nm and 0.34 at $\lambda_2 = 995$ nm, and an emissivity ratio of 1.09. Using these emissivity ratios for the solid and liquid phases, the measurement errors were generated against temperature and illustrated in Fig. 12.

4.2.1.2 Molybdenum There are also measured normal spectral emissivities of solid and liquid molybdenum determined at the wavelengths of 684.5 nm, 902 nm, and 1570 nm in the temperature range between 3000 K and 4800 K [4]. Similar to tungsten, the values show a less distinctive dependence on temperature, but an obvious effect by the wavelength as well as a noticeable downward step at the solid-to-liquid phase transition. Figure 13 shows three emissivity values measured for each of the solid and liquid phases averaging the merely small temperature dependence. As shown above, the emissivity was interpolated with the regression function at the two wavelengths, which were used for two-color pyrometry by the DPV-2000. The regression coefficient $a = -0.4551$ is again not far from -0.5 as expressed by the Hagen-Rubens law. For solid molybdenum, the interpolated emissivities are 0.45 at $\lambda_1 = 787$ nm and 0.41 at $\lambda_2 = 995$ nm with an emissivity ratio of 1.11 showing deviation from the gray-body assumption. For liquid molybdenum, the emissivities are 0.33 at $\lambda_1 = 787$ nm and 0.31 at $\lambda_2 = 995$ nm, and the emissivity ratio is 1.05. Using these emissivity ratios for the solid and liquid phases, the measurement errors generated as a function of temperature is shown in Fig. 14.

The estimates of the systematic temperature error due to the deviation of the emissivity characteristics from the gray-body assumption for solid tungsten and molybdenum are in good agreement with [7]. Here, the calibration of a two-color pyrometer working in the visible and near-IR range up to a wavelength of 1 μm is reported using tungsten and molybdenum samples, which were placed in an optically accessible heating and temperature measurement facility up to fusion temperatures. The calibration experiments showed that the systematic error induced by the deviation from the gray-body assumption is 50 K at 1600 K and almost 300 K at 3654 K.

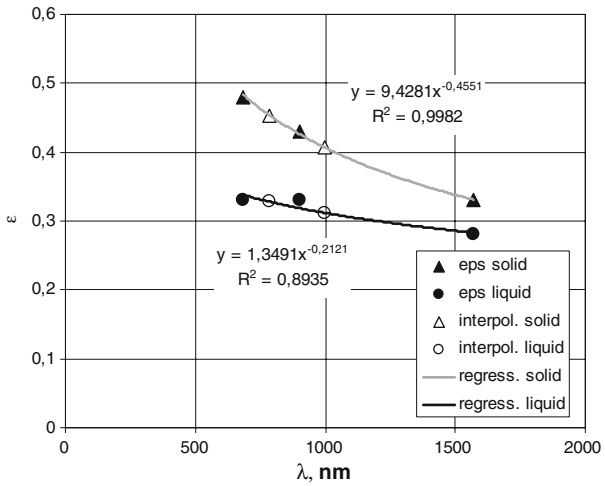

Fig. 13 Measured emissivity values taken from [4] (*filled circles*), regression functions (*black and gray lines*), and interpolated values at filtering wavelengths of DPV-2000 (*open circles*) for each the solid and liquid phases of molybdenum (eps means ε)

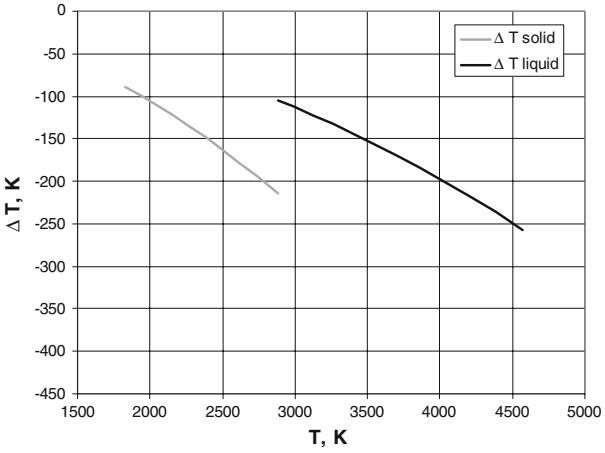

Fig. 14 Temperature measurement error caused by the deviation from the gray-body assumption for solid and liquid molybdenum

Furthermore, the emissivity characteristics of tungsten and molybdenum were found to be similar.

4.2.1.3 Yttria-Stabilized Zirconia (*YSZ*) Unfortunately, only very few references on emissivities of yttria-stabilized or pure zirconia are relevant for particle measurements by two-color pyrometry. Many investigations were carried out with emphasis on the performance of thermal barrier coatings and therefore, cover wavelengths in the µm range at comparatively moderate temperatures [8–10]. Most of the papers reported measurements of reflectivities. However, it is neither quantified how much of the

unreflected radiance energy is absorbed and re-emitted, nor how much is transmitted due to partial translucency. The latter is characteristic for zirconia in the wavelength range of up to approximately 8 µm [11], and is also found for other oxide ceramics, e.g., alumina [3].

Measurements of the non-hemispherical reflectivity of 8 mol% YSZ are reported at wavelengths of 480 nm, 630 nm, 1.15 µm, and 3.39 µm and at temperatures up to 3,100 K [12,13]. However, the quantitative values of the emissivity cannot be deduced, because the available transmittance is not quantified as well. The reflectivity decreases strongly with increasing temperature. Probably this is due to the scattering performance of the material which changes with the microstructure. The samples were produced by cold pressing and subsequent sintering at 2000 K and had a porosity between 18% and 20%. Hence, at elevated temperatures, further sintering effects can be expected. Moreover, the measurements show that at temperatures less than the melting point, the reflectivities in the visible and near-IR ranges become almost invariable with wavelength.

Measurements of the optical properties of plasma-sprayed YSZ thermal barrier coatings in the continuous wavelength range from 0.5 to 2.5 µm are reported in [14]. Transmittance and reflectance were measured by IR spectrometry. From this, the absorbance was calculated and compared to measured values obtained by photothermal deflection spectroscopy, which showed good agreement. All measurements were carried out at room temperature. Regarding two-color pyrometry of molten particles, however, the conditions are differing. The effect of the changing microstructure at high temperatures is not considered. At room temperature the porosity of the as-sprayed coatings determines vastly the scattering performance, which furthermore is wavelength-dependent.

There are also other references which indicate that the structure properties significantly affect the reflectivity [14]. Spectral directional hemispherical reflectance measurements of YSZ at elevated temperatures are reported in [15] over the wavelength range between 512 nm and 860 nm. They show an almost constant level against the wavelength, and a decrease with temperature from approximately 0.8 at 1200 K to approximately 0.5 at 2000 K. In contrast, after melting and re-solidification, the measured dependence of the reflectance with temperature is reversed (0.2 at about 1600 K and 0.4 at more than 2000 K). The authors assume microstructure and reduction/re-oxidation effects to be the reason for this. Other investigations on the impact of melting and subsequent solidification on the microstructure, and thus on the reflectivity of YSZ, can be found in [12,13].

The conclusion that can be drawn so far with regard to two-color pyrometry of pure or YSZ is that, at high temperatures beyond approximately 2500 K, the dependence of the emissivity on the wavelength in the visible and near-IR range is quite weak. Furthermore, the absolute emissivity values appear to be at a low level. Hence, the emissivity ratio and thus the measurement error are very sensitive to possible small changes of the emissivities. However, an attempt to quantify the emissivities more precisely at the wavelengths used by the DPV-2000 seems hardly reliable on the basis of the available data.

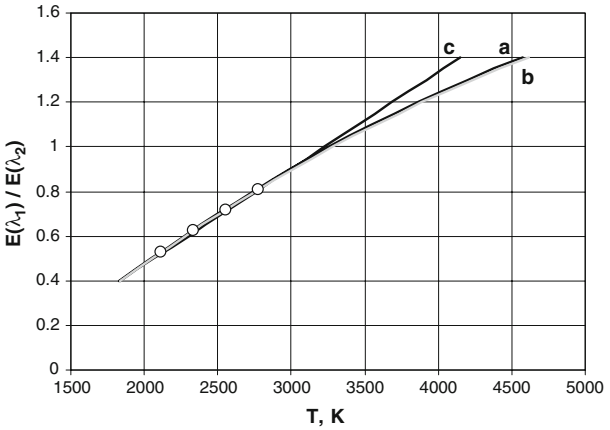

Fig. 15 Evolution of the relationship between the measured ratio of radiation intensities and temperature. Line (a) denotes the approximately exact relationships according to Wien's approximation of Planck's law. Line (b) shows a corresponding curve which was fitted to the four individual calibration points (marked by *circles*) of the applied tungsten ribbon lamp. Line (c) denotes the linear fit used by the DPV-2000

4.2.2 Calibration of the DPV-2000

To calibrate the DPV-2000 for temperature measurements, the sensor head was installed in a socket in front of a tungsten ribbon lamp. This lamp had been individually calibrated by the manufacturer prior to shipping using a high-precision pyrometer. A calibration sheet provided four temperatures and the appropriate currents and voltages. These calibration points were adjusted consecutively by a potentiometer, and the temperature for each was measured. Finally, a regression function was fitted to the measured data linking the measured intensity ratios with the temperature values given in the calibration sheet. Instead of the exact relationship according to Planck's law, the DPV-2000 works with a linear fitting function. This is acceptable within the temperature range by which the tungsten ribbon lamp can be operated. Here, between 1840°C and approximately 2500°C, Planck's law also results in an almost linear behavior. However, at higher temperatures, there is an increasing gap leading to significant systematic measurement errors.

Figure 15 shows the evolution of the relationship of the measured ratio of radiation intensities and temperatures. The blue line denotes almost exact relationships according to Wien's approximation of Planck's law. The red line shows a corresponding curve that was fitted to the four individual calibration points (marked by red dots) of the used tungsten ribbon lamp by introducing a correction factor which considers the different sensivities of the photodiodes in the sensor head. The green line denotes the linear fit with which the DPV-2000 worked. As shown in Fig. 16, at higher temperatures the measurement values are increasingly too low. For example, at the melting temperature of tungsten at 3683 K, the measurement error is −153 K.

It should be noted that this calibration considers mainly the different sensivities of both the photodiodes in the sensor head and is exactly valid only for the calibration lamp material and such others with similar emissivity characteristics. As shown

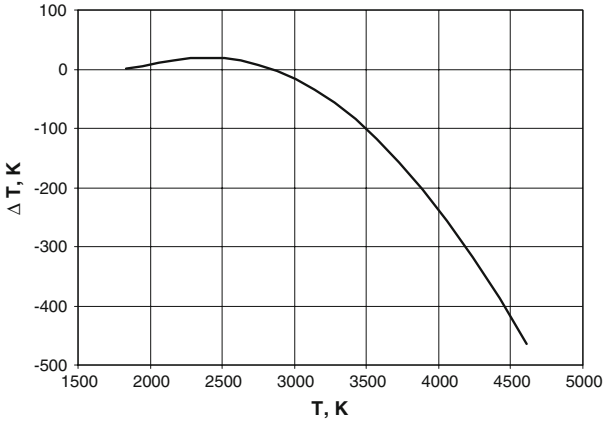

Fig. 16 Measurement error by using a linear fit instead of a curve in accordance to Wien's approximation of the Planck's law

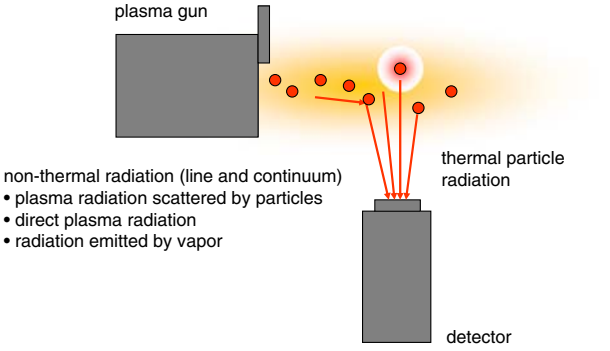

Fig. 17 Relevant non-thermal radiation sources potentially influencing the temperature measurement using two-color pyrometry

below, the emissivity characteristics of many other substances, such as that for the oxide ceramics, vary significantly from that of tungsten.

4.2.3 Non-thermal Radiation

Two-color pyrometry may be affected by interfering non-thermal radiation (line and continuum emission). Figure 17 shows the sources which greatly influence temperature measurements, namely [16–19]:

- Radiation emitted by the plasma,
- Radiation emitted by evaporated particle material and impurities, and
- Radiation coming from the plasma source being scattered by the particles.

As the optical sensor collects the total radiation including the non-thermal signals, the ratio of the measured intensities at the wavelengths used for two-color pyrometry may be distorted.

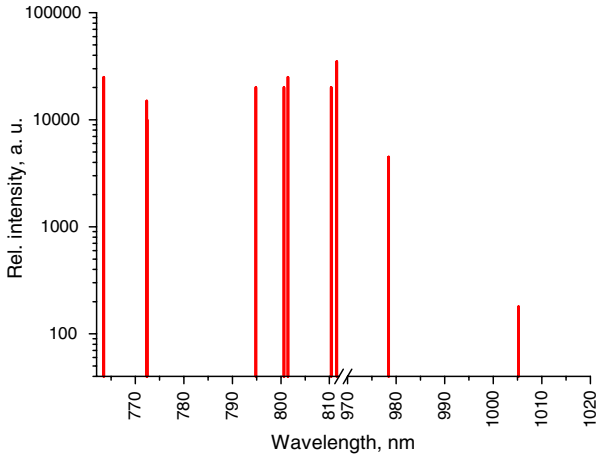

Fig. 18 Emission line spectrum of argon at the wavelength ranges of (787 ± 25) nm and (995 ± 25) nm; data taken from [20]

In principle, direct and scattered plasma radiation becomes significant, if the particle radiation is decreasing, i.e., at lower temperatures and at decreasing emissivities. Furthermore, the intensity of the plasma radiation is dependent on the excitation energy and the local gas concentration. Hence, the effect of non-thermal signals is especially large near the plasma torch exit and where there are few or relatively cool particles, such as those at the edges of the plume.

Regarding the line emission spectra of the plasma gas species and the particle materials considered here, only argon shows a few emission lines in the wavelength filter bandwidths used by the DPV-2000. Figure 18 shows the respective sections at $\lambda_1 = (787 \pm 25)$ nm and $\lambda_2 = (995 \pm 25)$ nm.

Experimental results [19] show that at plasma spraying conditions addressed above for tungsten, molybdenum, or YSZ, the effect of direct and scattered plasma radiation is to be expected negligibly low [19]. However, this is also coming from the proper selection of the filtering wavelengths of the DPV-2000. Thus, in the continuous wavelength range from 340 nm to 880 nm, the effect of particle-reflected plasma light can increase the argon line intensity up to 120%, which would induce a significant temperature measurement error [17]. The respective wavelength sections have to be necessarily filtered out as done by the DPV-2000.

Measurements between the wavelengths of 630 nm and 880 nm were reported, showing that the plasma radiation dominates the non-thermal radiance further downstream, while near the torch exit, vapor signals of the particle material are found to be significant [18]. By determining and subtracting the non-thermal signal from the collected spectra, more accurate particle temperatures could be achieved. Spraying molybdenum with +63 to 75 µm powder size at approximately 30 kW with an Ar–He plasma gas mixture, the accordant correction was low (1.5%) near the center of the radial particle distribution. At the edges of the distributions, the error was found to be largest at 14%.

Overall it can be expected that by using the DPV-2000 temperature measurements near the maximum particle flux at usual spraying distances are hardly affected by non-thermal radiation, provided that the particle radiation is sufficiently intense.

4.2.4 Radial Temperature Gradient and Semi-transparency of Particles

Along their trajectories, there is an intense heat exchange mainly by convection between plasma-sprayed particles and the ambient plasma gas. In most of the applications, it is required that the particles are fully molten and that the liquid state can be preserved until impinging onto the substrate. Regarding the particle characteristics, the time which is necessary to melt a particle completely by convectional heat transfer is dependent on the particle radius, the particle thermal conductivity, and the particle fusion enthalpy density [21,22]. Due to their higher thermal conductivity and lower fusion enthalpy, a metal particle melts faster than a ceramic particle of equivalent size. Spray parameters are usually designed to ensure that there is enough time to melt the particles completely.

Considering the heat flux through the interface between the ambient gas and the particle as well as inside the particle, a radial temperature gradient between the particle surface and center will develop which is steeper for ceramics than for metals. Approaching the substrate, the heat flux reverses and the particle cools again. This means that at a spraying distance, the core of the particle has a higher temperature than its surface.

Considering that oxide ceramics have a large wavelength range where they are distinctly semi-transparent, the temperature gradient within the particle could be of importance because the measured radiation partly originates from within the particle. Assuming that the particles' optical thickness is that of the product of the particle radius and the absorption coefficient, the measured temperature is principally not the surface temperature since it is obtained in opaque materials, but rather the temperature of an internal layer.

Estimates for YSZ show that the temperature difference within the particles is much higher when the particles are heated on the very first part of their trajectories [23]. However, approaching the substrate at the spraying distance, the inner temperature gradient is comparatively small. Figure 19 shows schematically the temperature development against the spraying distance for the surface and the core of a sprayed particle. Thus, the impact of semi-transparency and temperature distribution on the results of the two-color pyrometry is assumed to be negligible for common spray conditions.

4.3 Correction of Measured Melting Temperatures

Figure 20 shows the melting temperatures of tungsten and molybdenum from reference data [24] as compared to the experimental results which were obtained from DPV-2000 in-flight particle measurements. The analysis of these results shows distinct peaks in the particle distribution density curves which can be assigned to the melting

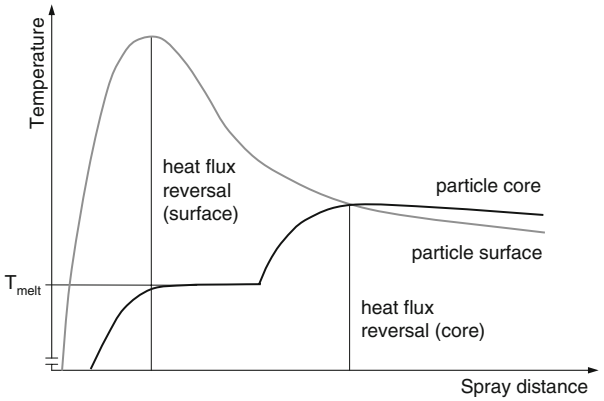

Fig. 19 Schematic temperature development as a function of the spraying distance at the surface and in the core of a sprayed particle

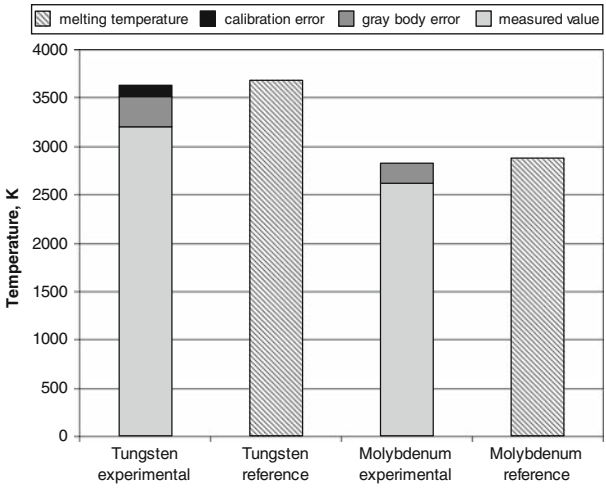

Fig. 20 Reference data for melting temperatures of tungsten and molybdenum [24] compared with corrected experimental results from DPV-2000 in-flight particle measurements

temperatures. Based on the emissivity data presented above, the measurement errors due to the deviations from the gray-body assumptions were calculated. Additionally, the error due to the linear calibration being significant only for tungsten was determined. Hereby, the measurement results were corrected. The best agreement with the reference data was obtained by using the emissivity data of the solid materials. This may indicate that the cooling particle surfaces at melting temperature were already solidified.

For YSZ similar DPV-2000 measurements were carried out. Here, distinct peaks in the distribution density curves could also be identified at approximately 300 K below the referenced melting temperature. Similar to molybdenum, the calibration error in this temperature range is negligible. The expected error due to the deviation from the

gray-body assumption should also be of smaller magnitude, because as previously shown, the dependence of the emissivities on the wavelength is assumed to be weak.

Therefore, other reasons for the difference between the reference and the experimental data are assumed to be present. Possibly, the measurement error is small, but the solidifying particles are undercooled. There are several references on undercooling effects in oxide ceramic particles. As already mentioned, liquid alumina droplets were found to be approximately undercooled by 240 K before solidification begins [3]. Especially for YSZ at plasma spraying conditions, several papers suggest that impinging particles in parts are largely undercooled about some hundred degrees [25–28]. Another possibility for explaining the differences between the reference and the experimental melting temperatures of YSZ is heat loss due to surface evaporation. However, this was not investigated experimentally.

5 Conclusions

Using two-color pyrometry, it is possible to collect in-flight single particle data during plasma spraying processes. The statistical analysis of the particle temperature distributions allows for the assessment of the melting status of the particles. In particular, the melting temperature and the particle fractions at the molten or already solidifying stage can be identified.

Using two-color pyrometry, relevant sources for measurement errors were identified to be due to the

- Deviation of particle material from a gray-body assumption,
- Calibration of DPV-2000.

For metals like tungsten and molybdenum, the gray-body error can be readily estimated and corrected. However, due to missing reliable emissivity data, this remains difficult for oxide ceramics like yttria-stabilized or pure zirconia.

The calibration error can be corrected for all materials. It is significant only at temperatures above 3000 K.

Acknowledgments Helpful discussions on application of particle diagnostics with L. Pouliot (Tecnar Automation Ltée, St-Bruno, QC, Canada) are gratefully acknowledged. The authors also would like to thank Dr. J.-L. Marqués-López for discussions on measurement results and Dr. M. O. Jarligo for editing of the manuscript.

References

1. J.R. Fincke, D.C. Haggard, W.D. Swank, J. Therm. Spray Technol. **10**, 255 (2001)
2. T. Streibl, A. Vaidya, M. Friis, V. Srinivasan, S. Sampath, Plasma Chem. Plasma Process. **26**, 73 (2006)
3. V. Sarou-Kanian, J.C. Rifflet, F. Millot, Int. J. Thermophys. **26**, 1263 (2005)
4. C. Cagran, G. Pottlacher, M. Rink, W. Bauer, Int. J. Thermophys. **26**, 1001 (2005)
5. H. Watanabe, M. Susa, H. Fukuyama, K. Nagata, Int. J. Thermophys. **24**, 223 (2003)
6. H. Madura, T. Piatkowski, Infrared Phys. Technol. **46**, 185 (2004)
7. S.P. Mates, D. Basak, F.S. Biancaniello, S.D. Ridder, J. Geist, J. Therm. Spray Technol. **11**, 195 (2002)
8. H. Tanaka, S. Sawai, K. Korimoto, K. Hisano, J. Therm. Anal. Calorimet. **64**, 867 (2001)
9. A. Ferriere, L. Lestrade, J.-F. Robert, J. Sol. Energ. – Trans. ASME **122**, 9 (2000)

10. Y.S. Touloukian, D.P. DeWitt, *Thermal Radiative Properties, Nonmetallic Solids, Thermophysical Properties of Matter*, vol. 8 (IFI/Plenum, New York/Washington, 1972)
11. J.I. Eldridge, C.M. Spuckler, K.W. Street, J.R. Markham, Ceram Eng. Sci. Proc. USA **23**, 417 (2002)
12. V.A. Petrov, A.Y. Vorobyev, A.P. Chernyshev, High Temp. High Press. **34**, 657 (2002)
13. F.A. Akopov, G.E. Val'yano, A.Y. Vorob'ev, V.N. Mineev, V.A. Petrov, A.P. Chernyshev, High Temp. **39**, 244 (2001)
14. A. Stuke, R. Carius, J.-L. Marqués, G. Mauer, M. Schulte, D. Sebold, R. Vaßen, D. Stöver, Optimizing of the reflectivity of air plasma sprayed ceramic thermal barrier coatings, in *31st International Cocoa Beach Conference on Advanced Ceramics and Composites*, Daytona Beach, Florida (2007)
15. S. Eckhoff, I. Alxneit, M. Musella, H.-R. Tschudi, Development of a reflectometer for the determination of the spectral emittance in the visible at high temperatures, in *PSI Scientific Report – Annex V* (Paul Scherrer Institut, Villigen, Switzerland, 2000), p. 26
16. P. Gougeon, C. Moreau, J. Therm. Spray Technol. **2**, 229 (1993)
17. K. Hollis, R. Neiser, J. Therm. Spray Technol. **7**, 383 (1998)
18. K. Hollis, R. Neiser, J. Therm. Spray Technol. **7**, 392 (1998)
19. Z. Salhi, P. Gougeon, D. Klein, C. Coddet, Infrared Phys. Technol. **46**, 394 (2005)
20. Yu. Ralchenko, F.-C. Jou, D.E. Kelleher, A.E. Kramida, A. Musgrove, J. Reader, W.L. Wiese, K. Olsen, NIST Atomic Spectra Database, Version 3.1.0, July 2006 (National Institute of Standards and Technology, Gaithersburg, MD), http://physics.nist.gov/asd3. Accessed 3 Jan 2007
21. H.-B. Xiong, L.-L. Zheng, L. Li, A. Vaidya, Int. J. Heat Mass Transfer **48**, 5121 (2005)
22. L. Li, A. Vaifya, S. Sampath, H. Xiong, L. Zheng, J. Therm. Spray Technol. **15**, 97 (2006)
23. L.A. Dombrovsky, J. Quant. Spectrosc. Radiat. Transfer **73**, 433 (2002)
24. I. Perry, D.W. Green, J.O. Maloney (eds.), *Perry's Chemical Engineer's Handbook*, 7th edn. (McGraw-Hill, New York, 1997)
25. Y.K. Chae, J. Mostaghimi, T. Yoshida, Sci. Technol. Adv. Mater. **1**, 147 (2000)
26. G.-X. Wang, R. Goswami, S. Sampath, V. Prasad, Mater. Manuf. Process. **19**, 259 (2004)
27. K. Shinoda, Y. Kojima, T. Yoshida, J. Therm. Spray Technol. **14**, 511 (2005)
28. K. Shinoda, T. Koseki, T. Yoshida, J. Appl. Phys. **100**, 1 (2006)